Published in final edited form as:
Dev Cell. 2014 December 22; 31(6): 690–706. doi:10.1016/j.devcel.2014.11.002.

The left-right *Pitx2* pathway drives organ-specific arterial and lymphatic development in the intestine

Aparna Mahadevan[1], **Ian C. Welsh**[1], **Aravind Sivakumar**[1], **David W. Gludish**[2], **Abigail R. Shilvock**[1], **Drew M. Noden**[3], and **Natasza A. Kurpios**[1,*]

[1]Department of Molecular Medicine, College of Veterinary Medicine, Cornell University, Ithaca, NY 14853, USA

[2]Department of Microbiology and Immunology, College of Veterinary Medicine, Cornell University, Ithaca, NY 14853, USA

[3]Department of Biomedical Sciences, College of Veterinary Medicine, Cornell University, Ithaca, NY 14853, USA

SUMMARY

The dorsal mesentery (DM) is the major conduit for blood and lymphatic vessels in the gut. The mechanisms underlying their morphogenesis are challenging to study and remain unknown. Here we show that arteriogenesis in the DM begins during gut rotation and proceeds strictly on the left side, dependent on the Pitx2 target gene *Cxcl12*. Although competent *Cxcr4*-positive angioblasts are present on the right, they fail to form vessels and progressively emigrate. Surprisingly, gut lymphatics also initiate in the left DM and arise only after – and dependent on – arteriogenesis, implicating arteries as drivers of gut lymphangiogenesis. Our data begin to unravel the origin of two distinct vascular systems and demonstrate how early L-R molecular asymmetries are translated into organ-specific vascular patterns. We propose a dual origin of gut lymphangiogenesis, where prior arterial growth is required to initiate local lymphatics that only subsequently connect to the vascular system.

INTRODUCTION

The vascular supply serving the highly coiled gut tube is structurally and functionally complex. While arteries and veins are largely congruent distally, proximally they separate in space and function, where the arteries connect dorsally to the aorta while veins drain ventrally into the hepatic portal system. This separation is present even before DM

*Author for correspondence: natasza.kurpios@cornell.edu, phone: 607-253-4452; fax: 607-253-3659.

Author contributions

N.A.K. and A.M. designed the research with additional contributions from D.M.N., D.W.G. and I.C.W; A.M. performed all the experiments, I.C.W., A.S., A.R.S contributed data (Fig. 4AC–H, Fig. S4E), (Fig. 2A–I, Movie S1–3), (Fig. 7F–I), respectively; D.M.N contributed technical expertise and tools, D.W.G. performed microarray data analysis. N.A.K, D.M.N. and A.M. wrote the paper.

formation, when the only vessel present is a single branch of the dorsal aorta: the cranial (superior) mesenteric artery (CMA). Only later as the DM expands during gut looping do additional arterial, then venous branches form in close association with the gut wall. This segregation of veins from arteries is essential and unique to the gut, and failure to remain fully separated causes portosystemic shunts and the metabolic imbalances that arise when blood drained from the gut bypasses detoxification in the liver (Gallego et al., 2002).

A rich network of lymphatic vessels is also present within the DM. Unlike peripheral lymphatics that follow veins, intestinal lymphatics parallel mesenteric arteries. While intestinal lymphatics are essential for immunity and fat absorption, their origin remains elusive (Heuer, 1909).

Like most vertebrates, humans have bilateral symmetry, with the majority of body systems more or less symmetric. Whereas the gut begins as a symmetrical midline tube, it later loops and rotates in a highly conserved, asymmetric pattern necessary for correct packing into the body cavity. To avoid strangulation of gut vessels, their development must be coordinated with the complex looping that characterizes gut morphogenesis (Fig. 1A). In mice and birds, this looping is driven by left-sided expression in the DM of the left-right (L-R) symmetry-breaking transcription factor *Pitx2* (Fig. 1AB, orange; Fig. 1D) (Davis et al., 2008). The chicken DM forms on day 2.5 (Hamburger-Hamilton [HH] stage 17, akin to mouse embryonic [E] day 10) (Hamburger and Hamilton, 1992) and consists of distinct cellular compartments that, via specific morphological changes, deform mechanically and swing the attached gut tube leftward. This tilt provides a bias for asymmetric gut rotation, disruption of which randomizes gut looping (Davis et al., 2008; Shiratori et al., 2006). Importantly, these asymmetries are short-lived, and once looping is underway, the wide, asymmetric DM transforms into a thin suspensory morphology with no observable L-R asymmetry (Savin et al., 2011).

To uncover mechanisms downstream of *Pitx2* that cause asymmetric cell behavior, we performed laser micodissection of the left and right DM (left: *Pitx2*-positive vs. right: *Pitx2*-negative, Fig. 1C), when L-R DM asymmetries are observed (Welsh et al., 2013). Unexpectedly, many of the genes with significant L-R differences are associated with arterial and lymphatic formation. Using live imaging, chick-quail chimeras, targeted in ovo misexpression, and transgenic mice we demonstrate in the DM the left-side restricted formation of transient arteries, which quickly remodel and join the CMA to become the permanent arteries supplying the midgut. To our surprise, gut lymphatics also initiate in the left DM and arise only after – and dependent on -arteriogenesis, implicating arteries as a driver of gut lymphangiogenesis. Finally, we demonstrate that the Cxcl12/Cxcr4 pathway is a target of Pitx2 necessary for vascular morphogenesis in the left DM. With these findings, we introduce a system to dissect in vivo the mechanisms that spatially pattern blood and lymphatic vessels of the vertebrate gut.

RESULTS

Arterial development in the DM is restricted to the left side

Microarray analyses of the L-R DM revealed that many differentially expressed genes were associated with endothelial vessel formation (Fig. 1C, Fig. S1), suggesting that vascular patterning was asymmetric in the gut. Among the top candidates were the arterial identity marker gap junction alpha-5 protein (*Gja5*), Notch pathway genes, and markers of haematopoietic cell clusters (*Cd34* and others, Fig. 1C, Fig. S1). RNA in situ hybridization (ISH, Fig. 1EF) using pan-endothelial (*PlexinD1*) or arterial endothelial probes (*Gja5*), identified arterial cords coursing dorso-ventrally (D-V) between the dorsal aorta (DA) and the gut vascular plexus (GP) at the onset of gut rotation (HH20). Significantly, these were present only on the DM left side, within the more densely packed *Pitx2*-positive left mesenchyme (Fig. 1EF, red dashed box; Fig. 1D, left-sided *Pitx2*). No cords were present on the right side within the dispersed mesenchyme (Fig. 1EF, black dashed box), a phenotype specific to the DM, as endothelial vesicles were present bilaterally in adjacent tissues dorsal to the DM (Fig. S1) and in the gut plexus (Fig. 1E, Fig. S1). This left-sided vascular bias was confirmed with quail endothelial-specific antibody QH1 (Fig. 1G, red) and transgenic *Tie1*:H2B-eYFP quail embryos (Fig. 1H, green, Fig. 1D, model).

The DM right side becomes avascular during gut rotation

The gut vascular system derives from incompletely identified progenitors (Pardanaud et al., 1989) that form a bilaterally symmetric endothelial plexus residing in the left and right splanchnic mesoderm (DM precursor) (Thomason et al., 2012). Thus, we hypothesized that existing right-sided endothelium must become excluded to generate the left-sided bias (Fig. 1E–H). Time series experiments revealed that, when the gut tube is still open (HH17), a bilateral Tie-1-positive endothelial plexus is present in the left and right mesenchymal compartments (Fig. 2AD, green and red arrow). Strikingly, at the onset of cellular asymmetries within the DM, endothelial cells within the right mesenchyme become progressively excluded (Fig. 2BE, red arrow). At HH19–20, when the leftward tilt has initiated, only the left-sided D-V endothelial cords remain (Fig. 2CF, green arrow).

Ex vivo time-lapse analyses in transgenic quail (Movies S1–3; Fig. 2G–I; Fig. S2) showed Tie1 positive cells leaving the DM right side at the time of the tilt (Movie S1 and S3), many of which crossed to the left side (Movie S2 and S3; Fig. 2I, red arrow). No TUNEL staining was detected in these cells or the entire DM, confirming that apoptosis does not contribute to endothelial cell loss (Fig. S2H–J). Therefore, whereas vascular development proceeds in the left DM, endothelial cells on the right emigrate, suggesting the right DM is not permissive to vascular development.

To further test this, we transplanted fragments of the right (GFP labeled) or left mesentery (RFP) from a donor quail at HH17–18, just prior to the right-sided vascular regression, into the head mesenchyme of recipient chickens at HH9/10 (Fig. 2J–M) (Feinberg and Noden, 1991). Donor quail endothelium from both the left and right sides emigrated from the grafts and populated nearby and distant blood vessels of hosts (Fig. 2N–Q, n=12/20 from left vs.

n=14/23 from right, p>0.9536). Thus, competent endothelial cells are present bilaterally, but in the right DM are unable to execute further development (Fig. 2R).

Left-sided D-V cords become the major arteries supplying the midgut and are driven by *Pitx2*

Gja5-positive D-V cords first appear coincident with DM formation and onset of gut looping (HH17–21, Fig. 3A, orange arrowheads, quantified in Fig. 3B, orange bars). At HH22, most cords remodel ventrally forming a new longitudinal arterial plexus at the junction of the DM and gut mesenchyme (Fig. 3A). Importantly, this plexus coalesces at HH23 forming a highly stereotypical, permanent artery that extends cranially connecting the future colon to the CMA (Fig. 3A, red arrow; formation quantified in Fig. 3B, red curve). This primary longitudinal artery (1°LA) becomes the ileocolic artery, the terminal branch of the CMA supplying the cecum, ileum, and appendix (human) in the adult. At this stage, three D-V arterial cords located caudally remain in the DM and do not remodel until HH25 (Fig. 3A, orange arrowheads at HH23; quantification in Fig. 3B). The left-sided bias for DM arterial remodeling and for the final position of the 1°LA was confirmed with subsequent transverse sections of *Gja5*-stained embryos (Fig. 3F).

At HH25, as the intestinal loop elongates ventrally (Fig. 3C, dashed arrow), the remaining D-V cords disappear, and a second arterial plexus forms that extends cranially and is positioned halfway between the terminal ileocolic branch point and the dorsal aorta (Fig. 3C, red arrowheads). This secondary longitudinal artery (2°LA) connects to the CMA by HH26 (Fig. 3C) and becomes the middle colic artery, the next branch of the CMA supplying the transverse colon. With further intestinal elongation, a third branch arises as an anastomosis between the ileocolic and middle colic arteries at HH29 (Fig. 3C). This right colic artery feeds the distal ascending and proximal transverse colon. Thus, vascularization of the intestine is accomplished in the left DM by asymmetric and transient assembly of multiple arterial D-V cords, followed by their remodeling into the permanent major arteries supplying the caudal half of the vertebrate midgut (Fig. 3D, left lateral view of embryo; Fig. 3E, slices of DM/gut tube).

The DM asymmetries are evolutionarily conserved among birds and mice and require left-sided *Pitx2*. We examined vascular development in *Pitx2*+/+, *Pitx2* +/− and *Pitx2*−/− mouse embryos, and found that, like chickens, wild type (WT) mice formed transient left-sided D-V arterial cords at E10.75 (Fig. 3G, Fig. S3), while reduced Pitx2 function in −/− and +/− embryos significantly decreased *Gja5*-positive cords in the DM (Fig. 3GH, n=5, $p = 0.0003$ +/+ vs. −/−, $p< 0.0052$ +/+ vs. +/−). Thus, *Pitx2* plays a necessary and conserved function during arterial patterning in the DM.

Asymmetric organization of the Cxcr4/Cxcl12 pathway across the L-R axis of the DM

Of specific interest to gut vasculogenesis is the chemokine *Cxcl12*, ligand for the receptor *Cxcr4*. Mice lacking *Cxcr4* or *Cxcl12* display defective DM arteriogenesis (Ara et al., 2005; Tachibana et al., 1998). Indeed, ISH at HH20 confirmed that *Cxcl12* is present in the left DM mesenchyme surrounding the endothelium (Fig. 4A). Prior to DM formation and gut closure (HH17), when the intervening bilateral endothelial plexus remains, *Cxcl12* is also

expressed bilaterally (Fig. 4C). *Cxcl12* expression subsequently develops D-V asymmetry in the left DM, with its highest concentration ventrally where the 1°LA forms at the DM-gut boundary (HH23, Fig. 4D). In contrast, *Cxcr4* expression was found in endothelium of the D-V arterial cords (Fig. 4B) and in the intervening vascular plexus bilaterally (Fig. S4A). At HH25, *Cxcr4* expression remained in left-sided 1°LA endothelium (Fig. S4B). This finding is consistent with previous work illustrating that, in mouse intestine, *Cxcr4* is expressed only in arterial endothelium.

The Cxcr4/Cxcl12 axis is downstream of Pitx2

Pitx2 is both necessary and sufficient to govern the molecular and cellular character in the left DM (Davis et al., 2008; Kurpios et al., 2008). In mice lacking *Pitx2*, the left DM fails to condense, all L-R DM asymmetry is lost and stereotypical gut looping is randomized. In chicken embryos electroporated with ectopic *Pitx2* on the right side (*Pitx2* misexpression), DM cellular asymmetries are also lost. The normally loose right mesenchyme is instead densely compacted like the left side (a ‘double-left’ phenotype).

To learn whether *Pitx2* is sufficient to drive *Cxcl12/Cxcr4* and vascular program in the DM, we misexpressed *Pitx2* and GFP on the right side at HH14 (Fig. 4E–L). GFP-positive cells were found only on the right side at HH20 (Fig. 4H), while GFP alone had no effect on vascular development (Fig. 4I–J). However, consistent with our previous work, *Pitx2* expressed on the right produced a ‘double-left’ phenotype including ectopic *Cxcl12* expression (Fig. 4F vs. E), ectopic formation of C*xcr4*- and *Gja5*- positive arterial D-V cords at HH20 (Fig. 4G, n=22/24; Fig. S4C), and two 1°LAs by HH21 (normal left and ectopic right, Fig. 4M, n=14/16).

Similarly, quantitative RT-PCR at E13.5 (Fig. 4N) and ISH at E12 (Fig. S4D) revealed a significant reduction in *Cxcl12* and *Cxcr4* expression in the DM of both Pitx2 +/− and *Pitx2*−/− mutant embryos (Fig. 4N, n=3, *Cxcl12*: $p = 0.0281$ +/+ vs. +/−, $p<0.018$ +/+ vs. −/−; *Cxcr4*: $p<0.004$ +/+ vs. +/−; $p<0.0005$ +/+ vs. +/−), showing that *Pitx2* regulates the Cxcl12/Cxcr4 axis and is necessary to initiate DM arteriogenesis.

To discern between direct and indirect Pitx2-dependent transcription, we confirmed Pitx2 binding sites at known Pitx2 targets and predicted conserved sites at the *Cxcl12* but not *Cxcr4* locus (Fig. S4E). These data agree with recently reported findings from in vivo ChIP-seq of FLAG-tagged Pitx2 binding in mouse cardiac tissue (NCBI Gene Expression Omnibus GSE50401) (Wang et al., 2014); we found five enriched Pitx2-binding peaks surrounding *Cxcl12*, one of which directly overlaps exon 1 of *Cxcl12* (Fig. S4E). No significant Pitx2 binding was observed at the *Cxcr4* locus arguing against a role for *Pitx2* expression in endothelial cells.

These data suggest that *Cxcl12* is a direct target of Pitx2 in vivo and that Pitx2-dependent *Cxcl12* expression in mesenchymal cells of the left DM signals to neighboring *Cxcr4*-positive (*Pitx2*-negative) endothelium to govern their behavior. Thus, Pitx2 appears to orchestrate a microenvironment permissive of vascularization, but does not autonomously determine endothelial cell fate decisions.

The Cxcr4/Cxcl12 axis is necessary for arterial development in the DM

To specifically address *Cxcl12/Cxcr4* function in the DM, we implanted beads soaked in a clinically validated Cxcr4 antagonist, AMD3100 (Matthys et al., 2001), into the left coelomic cavity prior to DM formation at HH14 (Fig. 5A). This had no effect on DM morphology or *Pitx2* expression (Fig. S5, n=6/6). However, it ablated both the *Gja5*-positive D-V cords (Fig. 5B, red arrows at HH21) and the 1°LA (Fig. 5C, red arrows at HH25, n=20/25, $p<0.0001$). AMD3100 effect was specific to the DM vasculature as other nearby channels including the gut plexus were unaffected (Fig. 5D, orange dashed lines, ISH *VE-cadherin*). Thus, the Cxcr4/Cxcl12 axis is necessary for local arterial development in the DM.

Cxcl12 expression is not sufficient to drive D-V cord formation in the absence of *Pitx2*

To learn whether *Cxcl12* can function in the absence of the L-R Pitx2, we targeted the Pitx2-negative compartment of the DM where D-V endothelial cords secondarily regress, and asked whether ectopic misexpression of *Cxcl12* can rescue this regression and support arterial vascular development in the absence of *Pitx2* (Fig. 6 and Fig. S6). As a control, we first overexpressed *Cxcl12* and GFP in the left, *Pitx2*-positive, DM, and performed spatiotemporal *Gja5* ISH on whole embryos to examine DM vascular processes upon ectopic *Cxcl12* overexpression. By comparison to the endogenous levels of left-sided *Cxcl12* in WT embryos, overexpression of *Cxcl12* on the left resulted in accelerated remodeling of D-V cords (Fig. 6ABC, gray vs. orange bars) and precocious formation of the left-sided 1°LA (HH18 with Cxcl12 vs. HH23 in WT embryos, red arrows in Fig. 6AC, red curve in Fig. 6B; n=25, $p<0.0001$). Transverse sections of these left side Cxcl12 electroporated embryos verified the left-specific targeting of the DM with GFP and confirmed the left-sided bias in the formation of this precocious 1°LA with ISH to *Gja5* (Fig. 6E, red arrow).

Next, we misexpressed *Cxcl12* and GFP in the right, Pitx2-negative, DM compartment and examined whether this can recapitulate the ‘double-left’ DM phenotype we routinely observe with ectopic *Pitx2* misexpression in the right DM (Fig. 4M). Unlike the isomerizing effects of *Pitx2*, right-sided *Cxcl12* produced normal L-R asymmetric DM morphology (Fig. S6A). Importantly, it was not sufficient to promote formation of ectopic D-V cords in the right DM at all stages examined (HH21 shown, Fig. 6E; note absence of cords in black dashed box; Fig. S6BA). Unexpectedly, in these *Cxcl12* (right side) electroporated embryos, an ectopic 1°LA developed on the right side at the mesentery/gut boundary on an accelerated timetable akin to left *Cxcl12* overexpression (Fig. 6ABD, purple vs. gray, $p>0.999$; Fig. 6E, red arrow; Fig. S6B). No left sided 1°LA was formed in these embryos (Fig. 6E and Fig. S6B).

Based upon these findings, we hypothesized that in the embryos electroporated with *Cxcl12* on the right, the ectopic levels of Cxcl12 overcame the chemotactic index of WT Cxcl12 on the left, prompting endothelial cell migration toward the right side, and contributing to the formation of a right-sided 1°LA (Fig. 6E, cartoon). Consistent with our hypothesis, *Cxcr4*-positive endothelial cells were found in the 1°LA induced by ectopic (right sided) *Cxcl12* (Fig. S6B, row 4). Furthermore, ISH for *Cxcl12* expression in electroporated embryos

revealed significantly higher levels of the ectopic right-sided *Cxcl12* by comparison to the endogenous levels of *Cxcl12* found on the neighboring left side (Fig. S6A).

To directly test this hypothesis, we performed a dual-targeting experiment to inhibit the formation of the left-sided *Cxcr4*-positive D-V cords and at the same time provide the right side with an ectopic source of overexpressed *Cxcl12* (Fig. 6F). If 1°LA formation requires the preceding transient D-V cords within the left *Pitx2*-positive DM compartment, an ectopic right-sided 1°LA should not develop in these *Cxcl12* (right side) electroporated embryos (Fig. 6F1). AMD3100-soaked (Fig. 6F1), or PBS (Fig. 6F2) beads were implanted on the left to inhibit normal D-V cord formation as described above, and in the same embryo *Cxcl12* was electroporated on the right. Compared to PBS bead controls (Fig. 6F2, n=7/7), Cxcr4 inhibitor-beaded embryos formed neither the normal left, nor an ectopic right 1°LA (HH25, Fig. 6F1, n=7/11, $p<0.0128$), consistent with our hypothesis that only the left-sided endothelial cells are able to form the 1°LA. As expected, electroporating *Pitx2* instead of *Cxcl12* on the right with the left side inhibited was able to support arterial development in the right DM, independent of the left side (Fig. 6F3), n=14/14, $p<0.0007$). As a technical note, the diffusion range of AMD3100 inhibitor does not extend beyond the midline boundary of the DM: inhibitor beads placed on the right side of WT embryos have no effect on the normal left-sided vascular assembly of cords and the 1°LA (Fig. S6C, n=17/17, $p<0.001$).

These findings suggest that *Cxcl12* expression guides the location of *Cxcr4*-positive arterial endothelial cells in the DM as a necessary angiogenic signal. 1°LA formation requires the preceding transient left D-V cords, a process dependent on the Cxcl12/Cxcr4 axis. Although necessary, Cxcl12/Cxcr4 signaling is not sufficient for this process indicating that Pitx2 must provide the critical framework, distinct from those of the adjacent gut vasculature, within which Cxcl12 can function.

Lymphangiogenesis in the DM is left-sided

Early studies supported by recent lineage tracing methods proposed that lymphatics are modified veins and originate from primary lymph sacs (centrifugal model) (Sabin, 1902; Srinivasan et al., 2007). An alternative model proposed that lymphatic vessels develop from mesenchymal precursor cells, independent of veins, and secondarily establish venous connections (centripetal model) (Huntington and McClure, 1910). In the dorsal regions of the abdomen, an unpaired retroperitoneal sac forms from subcardinal veins (SCVs) lying ventral to the aorta beside the root of the mesentery (dorsal margin of the DM, Figure S7). Early 20th century embryologists noted that gut lymphatics are first evident as centrifugal branches from the retroperitoneal lymph sac after E14 and proposed it to be the sole source of gut lymphatic vessels (Heuer, 1909). However, recent studies in mice have identified mesenchymal cells with lymphatic endothelial characteristics residing locally within the gut tube mesenchyme, far ventral to the retroperitoneal sac. These data suggest an alternative origin of intestinal lymphatics (Buttler et al., 2006; Pudliszewski and Pardanaud, 2005).

Because gut lymphatics course with arteries (not veins), we hypothesized that local mechanisms in the left DM that initiate arteriogenesis might similarly induce lymphangiogenesis. We initially detected no *Lyve1* or *Prox1* positive cells in the chicken

DM at HH20 when arterial D-V cords are still present (Fig. 7AB, red arrowheads). Both lymphatic markers were weakly expressed in the walls of the left and right SCV located beside the root of the mesentery (Fig. 7A). *Lyve1* was also weakly expressed throughout the midgut vascular plexus (Fig. 7A, GT) as shown in the mouse counterpart. Hence, at the onset of gut rotation, lymphatic precursors are resident in two distant locations: dorsal and ventral to the DM. Strikingly, by HH23, and coincident with the formation of 1°LA from D-V cords (Fig. 7CD, red arrows), we identified a robust plexus of *Lyve1*-positive cells in the left DM. These are first evident ventrally, then extend dorsally through the left DM mesenchyme (HH24) (Fig. 7C, green arrows). This pattern was confirmed with *Vegfr3* staining (Fig. 7C) and left lateral views of embryos at HH23 (Fig. 7E, green arrow) revealed a *Vegfr3*-positive vascular plexus present longitudinally along the mesentery/gut border and parallel to the 1°LA (Fig. 7E, red arrow).

At HH26, as the gut loop elongates, the initially wide, short DM transitions into a thin and long structure to accommodate the rapid gut elongation (Savin et al., 2011). This stage is characterized by the formation of the second arterial branch (2°LA) from the remaining D-V arterial cords (Fig. 7E, *Gja5*). Coincident with 2°LA formation, we observed that the *Vegfr3*-positive plexus extends dorsally within the left DM (Fig. 7E, green arrow) and towards the 2°LA (Fig. 7E, 2°LA; Fig. 7E, green arrow). It remains connected with the gut vascular plexus ventrally and grows new lymphatic cords dorsally that subsequently connect with the right SCV (Fig. 7E, green arrowheads). At HH26, we found *Prox1* only in the SCVs, indicating that not all lymphatic precursor cells are *Prox1*-positive at this stage, consistent with recent studies (van Impel et al., 2014) (data not shown).

At HH27, we detected *Prox1* expression in a sub-population of *Vegfr3*-positive endothelial cells that continues extending from the gut vascular plexus dorsally and within the left DM (Fig. 7FG, adjacent sections, green dashed box, Fig. S7B). *Prox1* was also expressed strongly in the avian-specific Nerve of Remak, and was distinguished from lymphatic populations by staining for the neural marker Hnk-1 (Fig. 7H, Fig. S7B, right column). *Prox1* expression was maintained in the dorsal region of the abdomen in an endothelial sub-population of the left and right SCV and also in a region ventral to the right SCV marked with *Vegfr3*-positive cells (Fig. 7FI, blue dashed box).

Similarly, in WT mice, wholemount immunohistochemistry (IH) and subsequent tissue sections revealed the first appearance of a Prox1-positive lymphatic vascular plexus at E10.5 in the ventral left DM (Fig. 7J, Fig. S7C). We confirmed the lymphatic identity of this population using *Prox1*-GFP transgenic mice (Choi et al., 2011) (Fig. 7K) and double-IH to the lymphatic endothelial marker Nrp2. These experiments revealed that the *Prox1* promoter is transcriptionally active in both dorsal (subcardinal vein, blue dashed box in Fig. 7KL) and ventral (left DM, green dashed box in Fig. 7KLM) locations within the DM. No *Prox1*-GFP-labelled cells were detected in the gut DM prior to E10.5 (Fig. J, Fig. S7C). Thus, *Prox1*-positive lymphatic precursors are resident in two separate locations in two model organisms: in the dorsal region of the abdomen (SCVs and dorsal margin of the DM) and in the ventral region of the left DM (Fig. 7N). These results show that gut lymphatics exhibit a left-sided bias, implicating the role of *Pitx2* during organ-specific lymphangiogenesis.

Pitx2 is required for lymphatic development in the mouse DM

To demonstrate the role of *Pitx2* during lymphatic development, we initially assayed for *Prox1* expression in WT and *Pitx2* mutant whole intestines using quantitative RT-PCR. Because *Pitx2*−/− embryos die at E14.5 (Lu et al., 1999), analyses were performed at E13.5. *Prox1* expression was significantly reduced in *Pitx2*−/− (Fig. 8C, n=5, p<0.0007) and *Pitx2*+/− mutant intestines (Fig. 8C, n=5, p<0.0083). We next performed ISH and double-IH for Prox1 and the pan-endothelial marker platelet-endothelial cell adhesion molecule-1 (Pecam-1) in WT and *Pitx2* mutant embryos. Consistent with a previous report (Wigle and Oliver, 1999), *Prox1* expression was seen in lymphatic vessels of the DM at E13.5, which connect ventrally with the gut plexus and dorsally with the lymphatic plexus found alongside the CMA (Fig. 8AB, arrow). Importantly, Prox1 expression was absent from all *Pitx2*−/− mutant mesenteric lymphatics at E13.5 (Fig. 8AB, asterisk), suggesting a lack of lymphatic vessels in the *Pitx2*−/− mouse DM. Strikingly, expression of *Prox1* in the lymphatic population alongside the CMA remained unchanged in *Pitx2*−/− embryos (Fig. 8A, arrowhead), highlighting that this lymphatic endothelium is *Pitx2*-independent. We obtained identical results with *Vegfr3* expression in WT and *Pitx2*-null embryos (Fig. S8A). Furthermore, we observed no phenotype in the formation of dermal lymphatics that arise from the paired jugular lymph sacs (Fig. 8B, insets), a process halted in *Prox1* null mice (Oliver, 2004). Hence, the organ-specific lymphatic phenotype in *Pitx2* null mice is distinct from that reported with *Prox1* loss of function, where all lymphatic structures are absent including those alongside the CMA (Wigle and Oliver, 1999).

These data demonstrate the existence of a separate population of lymphatic progenitors with distinct molecular and fate identity that forms local mesenteric lymphatic vessels and is dependent on the asymmetric expression of *Pitx2*.

Local lymphangiogenesis in the left DM requires the preceding Pitx2-driven arterial program

To begin addressing mechanisms that might be responsible for lymphangiogenesis in the DM, we blocked arterial formation by implanting Cxcr4/Cxcl12-inhibiting AMD3100 beads on the left side. Neither the *Lyve1*- (Fig. S8B) nor the *Vegfr3*-positive lymphatic network developed (Fig. 8D, middle, n=14/19, p<0.0001, orange dashed lines), suggesting that lymphangiogenesis in the DM requires prior arteriogenesis or is dependent on Cxcr4/Cxcl12. Similarly, Prox1/Pecam-1 expression was absent from all *Cxcr4*−/− mutant mouse mesenteries (Fig. S8C).

To uncouple arterial function from the Pitx2-driven Cxcr4/Cxcl12 axis we specifically blocked arteriogenesis with a validated Gja5 blocker, quinidine (Picoli et al., 2012). As expected, no *Gja5*-positive 1°LA formed in quinidine-beaded embryos (HH24, Fig. 8E, red arrow, n=6/9, p<0.0045) independent of *Cxcl12* expression (Fig. S8D). Importantly, quinidine completely ablated the *Vegfr3*-positive lymphatic network (Fig. 8D, right, orange dashed lines, n=17/25, p<0.0001). Consistent with our *Pitx2*−/− mice data, quinidine had no effect on *Vegfr3* expression in the chicken lymphatic population alongside the CMA (Fig. 8D, right, arrowhead, n=18/18). Thus, mesenteric lymphatic vasculature forms asymmetrically and is dependent on the prior assembly of the arterial vascular network in

the left DM, a process downstream of *Pitx2*. These primitive lymphatics subsequently extend dorsally to connect with centrifugal branches of the systemic vascular system (Fig. 8F, model).

DISCUSSION

We have leveraged the DM as a genetically accessible in vivo model to characterize vascular development in the intestine. Our work demonstrates that 1) arteriogenesis in the midgut is commensurate with the onset of gut rotation and proceeds strictly on the DM left side; 2) subsequent lymphangiogenesis is left-sided and is dependent upon, arteriogenesis; and 3) *Pitx2* and its target gene *Cxcl12* drive the formation of vascular channels in the DM, but *Cxcl12* alone is insufficient in the absence of a *Pitx2*-induced microenvironment. Our findings shed light on possible mechanisms by which L-R signaling determines organ-specific blood vascular and lymphatic situs throughout the embryo.

Pitx2 patterns blood vessels of the dorsal mesentery

Our work demonstrates that Pitx2-dependent processes directing initial gut rotation are also employed for patterning the vasculature within the midgut DM, and thus provide a mechanism to coordinate these two critical morphogenetic processes. Multiple mesenteric arteries form transiently on the left side of the DM, then remodel ventrally to form the permanent arterial branches of the CMA: the most distal (ileocolic) branch forms first, and as the loop herniates a second (middle colic) branch forms, ultimately giving rise to the third (right colic) branch as an anastomosis between the ileocolic and middle colic arteries. Interestingly, we observed no vascular events in the cranial half of the midgut at the time of rotation suggesting that vascularization of the proximal ileum and jejunum is temporally and spatially distinct from the large intestine. Indeed, the vascular pattern of the adult jejunum compared to other midgut-derived regions reflects this difference and is a consequence of the additional complex looping events in this segment (Savin et al., 2011).

Other asymmetric vascular events are similarly *Pitx2*-dependent, such as aortic arch remodeling (Yashiro et al., 2007), patterning of the azygos and portal veins (Shiratori et al., 2006) and the asymmetric branches of the celiac artery around the stomach, spleen and pancreas (Hecksher-Sorensen et al., 2004). Recognizing that local cues and effectors may differ among organs, our findings underline a conserved mechanism for organ-level vessel patterning in the viscera, and invite analysis of other known vascular asymmetries.

It is important to note that inhibition of vessel assembly on the right, *Pitx2*-negative side, is unique to the DM and necessary to limit mesenteric vasculogenesis to a singular process (not paired as occurs in the gut wall and mesonephros). This may be related to the early exclusion of veins from the DM, to prevent shunts between post-hepatic vitelline (portal) and systemic veins.

Cxcr4/Cxcl12 axis as a target of *Pitx2* during organ-specific vascular development

Our studies begin to address why the essential functions of Cxcl12 are organ-specific and why only arterial, not venous, endothelial cell populations require this pathway (Ara et al., 2005). We show that *Cxcl12* is a direct target of Pitx2 in vivo; Pitx2 restricts *Cxcl12*

expression to mesenchymal cells within the left DM, where it attracts neighboring *Cxcr4*-positive endothelial cells thereby directing asymmetric arteriogenesis. Although necessary, Cxcl12/Cxcr4 signaling can only operate effectively in the context of a Pitx2-induced microenvironment, indicating that additional factors are required. A strong candidate is Glypican 3 (Gpc3), the product of a gene mutated in Simpson-Golabi-Behmel syndrome, which causes complex vascular and gastrointestinal anomalies including gut malrotation (Pilia et al., 1996). Cxcl12 can bind heparin and heparan sulfate (Uchimura et al., 2006), which is thought to concentrate an otherwise diffusible ligand to form a durable chemotactic gradient (Bulow and Hobert, 2006; Lortat-Jacob, 2009). *Gpc3* expression in the gut DM mirrors the left-sided *Pitx2* and *Cxcl12* and forced *Pitx2* expression on the right induces *Gpc3* (Welsh et al., 2013).

We observed bilateral expression of *Cxcl12* in the left and right splanchnic mesoderm prior to DM formation (HH17) suggesting that this transient right-sided *Cxcl12* is Pitx2 independent. There have been other factors reported to regulate *Cxcl12* and include the canonical (Tamura et al., 2011) and non-canonical Wnt signaling (Tamura et al., 2011; Witze et al., 2008), Hypoxia-inducible factor-1 and 2 (Ceradini et al., 2004; Martin et al., 2010), and VegfA (Hong et al., 2006). Hence, some of these factors may also be responsible for regulating *Cxcl12* expression independent of Pitx2.

Previous work in zebrafish has shown that endothelial expression of *Cxcl12a/b* in major blood vessels directs formation of a spatially parallel trunk lymphatic network alongside preexisting blood vasculature (Cha et al., 2012). Thus, the interaction of lymphatic precursors with established arterial vessels likely represents a conserved mechanism of lymphangiogenesis, a process that could shed light on the etiology of diseases associated with lymphatic dysfunction. This correlation might further augment our understanding of the angiogenic influences of the Cxcr4/Cxcl12 chemokine axis in several inflammatory diseases including IBD (Alexander et al., 2010; Dotan et al., 2010). Indeed, polymorphism within exon 2 of human *Cxcr4* is associated with susceptibility to IBD (Mrowicki et al., 2014).

The embryonic origin of intestinal endothelial cells

Gasparo Aselli discovered lymphatic vessels in the dog mesentery nearly four centuries ago (Aselli, 1627), but the factors governing genesis of these channels remain uncertain. Multiple studies have shown that axial lymphatic vessels originate from lymph sacs; these include seminal work by Sabin (Sabin, 1902) and are supported by recent mammalian linage tracing and live imaging in zebrafish, demonstrating that lymphatic endothelial progenitors derive from primary lymphatic sacs, of venous origin (Srinivasan et al., 2007; Yaniv et al., 2006). An alternative theory pioneered by Huntington and McClure (Huntington and McClure, 1910) proposed that while lymph sacs might be of venous origin, peripheral lymphatics arise from local lymphangioblasts at a great distance from the lymph sacs, establishing the dual origin paradigm that remains today (Buttler et al., 2006; Ny et al., 2006; Papoutsi et al., 2001; Pudliszewski and Pardanaud, 2005; Wilting et al., 2006; Wilting et al., 2007; Wilting et al., 2000).

We find *Lyve1-*, *Prox1-*, *Vegfr3-*, *and Nrp2*-positive lymphatic precursors in the walls of the left and right subcardinal veins (SCVs) located dorsally beside the root of the mesentery. At

HH26, subpopulations of endothelial cells from the right SCV move ventrolaterally towards the right side of the dorsal DM towards the caudal side of the CMA (Fig. S7B), suggesting that these cells are the precursors of the retroperitoneal lymph sac, observed in the current study and elsewhere to descend from the right SCV, and together support the view of a venous origin for primary lymphatic sacs (Heuer, 1909). Importantly, this dorsally-derived population is Pitx2 independent, as *Prox1*- and *Vegfr3*-expressing cells were maintained alongside the CMA in *Pitx2* knockout mice.

However, our study identifies an additional population of lymphatic progenitors conserved in both the chicken and mouse within the ventral left DM and separated spatially from the SCV and temporally from the formation of the retroperitoneal lymph sac (Mouta-Bellum et al., 2009; Oliver, 2004). We show that the appearance of these *Lyve1*-, *Vegfr3*-, and subsequently *Prox1*-expressing cells requires the prior *Pitx2*-dependent assembly of arterial mesenteric blood vasculature. Importantly, while *Prox1*-null mice lack all lymphatics, including the retroperitoneal lymph sac and those of the gut (Wigle and Oliver, 1999), *Pitx2* knockout mice lack Prox1-positive mesenteric lymphatics but retain Prox1 expression alongside the CMA, suggesting an organ-specific role for *Pitx2* during gut mesentery lymphangiogenesis. The existence of a distinct program for intestinal lymphangiogenesis is further supported by the recent finding that mice lacking the phosphoinositide-3-kinase (PI3K) regulatory subunit 1 alpha (Pik3r1) (Mouta-Bellum et al., 2009) show severe lymphangiectasia specifically in the intestine, a phenotype that was independent of the retroperitoneal lymph sac.

Taken together, our results provide genetic evidence in support of at least two functionally and molecularly distinct lymphatic precursor populations in the intestine. The cellular origins of these populations are currently unknown and remain under examination using lineage tracing methods. Our work is consistent with the proposed dual origin of lymphatics and supports the principles of local embryonic lymphangiogenesis, which seem to be conserved among species and tissues. Understanding the developmental mechanisms responsible for organ-intrinsic lymphangiogenesis is important, as distinct lymphatic endothelial populations will likely contribute differentially to disorders of this exquisite organ system.

EXPERIMENTAL PROCEDURES

Animals

Embryos were collected from *Pitx2*^{hd} (Lu et al., 1999) and *Pitx2*$^{\Delta ASE}$ (Shiratori et al., 2006) mutant mice, Cxcr4-null mutant mice (Tachibana et al., 1998), *Prox1*-GFP transgenic mice from MMRRC (UC Davis), eggs of White Leghorn chickens (Sunrise), Japanese (Strickland) or transgenic *Tie1*-H2B-YFP quails (Ozark) at appropriate stages. Experiments adhered to guidelines of the Institutional Animal Care and Use Committee of Cornell University, under the Animal Welfare Assurance on file with the Office of Laboratory Animal Welfare.

Laser capture microdissection

Detailed methods are in preparation to be published elsewhere. Briefly, cryosections of unfixed/flash frozen WT HH21 chicken DM were arrayed on membrane slides (Leica, 11505189). The asymmetric morphology of the left and right DM was used to discriminate and capture separately each of four compartments. A contrast stain (HistoGene Kit, Arcturus, KIT0419) was applied just prior to LCM. GeneSpring-generated expression levels for Pitx2 (left) and Tbx18 (right, control) provided initial validation of dissections and analyses (Welsh et al., 2013).

In ovo targeting and quail-chick transplants

Avian embryos were electroporated with pCAG-GFP or –mCherry (HH14), using 5×10ms pulses of 30V (Welsh et al., 2013). Slices of HH20 quail embryos (150μm, Vibratome 800, McIlwain) were dissected into ~50×50×150μm GFP− or RFP+ pieces, and grafted into surgical excavations of the mesenchyme abutting the midbrain of HH9–10 chicken hosts (Noden, 1988). For pharmacological inhibition of Cxcr4, vehicle (PBS) or 5mg/ml AMD3100 (A5602, Sigma) was adsorbed onto AG beads (143–1255, Bio-Rad) overnight at 4°C. For inhibition of Gja5, vehicle (DMSO) or 40mM quinidine (22600–10G–F, Sigma) was adsorbed onto AG beads overnight at room temperature. The beads were placed into the coelom through an opening in the ectoderm and somatic mesoderm made with fine forceps. Dual targeting was performed by DNA microinjection and electroporation to first target the left splanchnic mesoderm (Welsh et al., 2013) (HH14), followed by the placing of inhibitor beads (HH16).

Histochemical analyses

Embryos were processed for immunohistochemistry (IH) on sections (Welsh et al., 2013) or wholemount IH (Betterman et al., 2012). Antibodies included: QH1 (DSHB), GFP (ab290, Abcam), RFP (Rockland, 600-401-379), N-term Prox1 (AF2727, R&D), PECAM (CD31, 553371, BD Bioscience), HNK1/CD57 (C6680, Sigma), Nrp2 (A567, R&D) and AlexaFluor anti-goat, anti-mouse or anti-rabbit 568, anti-rabbit 488, and streptavidin 594 conjugates. Images were taken using a Zeiss Observer.Z1/Apotome or Discovery.V12 microscope with AxiocamHRc, CoolSNAP HQ^2 or MYO cameras. Confocal images were taken in a Leica TCS SP5 system using a Plan Achromat 20X/0.7 objective. TUNEL was performed using the in situ cell death detection kit (Roche, 12156792910).

Statistical Analysis

D-V cords were counted and percent formation of the 1°LA was calculated as total length formed/length spanned by 7 somites caudal to the CMA (midgut region). JMP Pro 10.0 was used to generate means with Student’s t-test (Fig. 6B, 4N, 8C), Tukey-Kramer HSD test for multiple pair-wise comparisons (Fig. 3H), Fisher’s Exact test for inhibitor and dual-targeting data and Pearson’s Chi-squared test for quail-chick transplant data; error bars are standard error of the mean.

Explant culture and live imaging

Midgut slices of 200μm (HH17 *Tie*1:H2B-YFP quails) were made using Vibratome 800, (McIlwain). Explant live imaging was adapted from (Gros et al., 2010Gros et al., 2010; Heller et al., 2014). Briefly, midgut explants were suspended in warm recovery media (F12, 10mM HEPES, 1% Pen-strep; Invitrogen) and sealed against a matTek glass- (Movie S1 and S2) or Lumox Teflon-bottom dish (Sarstedt) (Movie S3) using a small volume of 1% low melting point agarose/F12. Images were captured every 7 minutes for 18 hours on a Zeiss LSM 780/Plan-Apo 20×/0.8 setup in an air- and stage-heated 5% CO_2 (Movie S3) or for periods of 6–10 hours using a Leica SP5/Plan-Apo 20×/0.7 setup in a heated, 5% CO_2 (Movie S1 and S2).

Image Analyses

Imaris 7.6.1 (Bitplane) was used for filtering, background subtraction and for transformation of confocal image stacks into volume-rendered four-dimensional movies. Nuclei were segmented in 3D, labeled with spot objects and tracked by manually specifying the nuclei location for each time point. Tracks were visualized with dragon tails (Movie S1 and S2), showing the object path over the previous 20 frames. This was verified with ImageJ. All movies were compiled using Adobe Premiere Pro.

Quantitative Real-Time PCR

Total RNA was extracted from resected whole gut (including mesentery and vasculature) of E13.5 mouse embryos using RNeasy Mini Plus (Qiagen), and subject to cDNA synthesis using the ABI High Capacity cDNA RT kit. TaqMan probes (Applied Biosystems; Cxcl12-Mm00445553_m1, Cxcr4-Mm01996749_s1, Pitx2-Mm00440826, Prox1-Mm00435969_m1) were used to quantify transcript abundance using the Applied Biosystems 7500, normalized to ß-Actin levels. JMP Pro 10.0 was used to calculate means using the Student's t-test.

Supplementary Material

Refer to Web version on PubMed Central for supplementary material.

Acknowledgments

We thank Drs. G. Oliver, N. Harvey, J. Martin, H. Hamada, T. Nagasawa, A. Bandyopadhyay and J. Sen for reagents described above. We are grateful to Drs. R. Lansford, D. Huss and D. Koos for imaging expertise as well as T. Wu, and C. Ly for technical assistance. This work was supported by the Cornell Center for Vertebrate Genomics (A.M.); NIH institutional support for I.C.W. (HD057854); March of Dimes 1-FY11–520 (N.A.K.); and NIH R01 DK092776 (N.A.K.).

References

Alexander JS, Chaitanya GV, Grisham MB, Boktor M. Emerging roles of lymphatics in inflammatory bowel disease. Annals of the New York Academy of Sciences. 2010; 1207(Suppl 1):E75–85. [PubMed: 20961310]

Ara T, Tokoyoda K, Okamoto R, Koni PA, Nagasawa T. The role of CXCL12 in the organ-specific process of artery formation. Blood. 2005; 105:3155–3161. [PubMed: 15626744]

Aselli, G. De lactibus, sive Lacteis venis, quarto vasorum mesaraicorum genere novo invento dissertatio. Medioloni, Milan; 1627.

Betterman KL, Paquet-Fifield S, Asselin-Labat ML, Visvader JE, Butler LM, Stacker SA, Achen MG, Harvey NL. Remodeling of the lymphatic vasculature during mouse mammary gland morphogenesis is mediated via epithelial-derived lymphangiogenic stimuli. The American journal of pathology. 2012; 181:2225–2238. [PubMed: 23063660]

Bulow HE, Hobert O. The molecular diversity of glycosaminoglycans shapes animal development. Annu Rev Cell Dev Biol. 2006; 22:375–407. [PubMed: 16805665]

Buttler K, Kreysing A, von Kaisenberg CS, Schweigerer L, Gale N, Papoutsi M, Wilting J. Mesenchymal cells with leukocyte and lymphendothelial characteristics in murine embryos. Developmental dynamics: an official publication of the American Association of Anatomists. 2006; 235:1554–1562. [PubMed: 16502417]

Ceradini DJ, Kulkarni AR, Callaghan MJ, Tepper OM, Bastidas N, Kleinman ME, Capla JM, Galiano RD, Levine JP, Gurtner GC. Progenitor cell trafficking is regulated by hypoxic gradients through HIF-1 induction of SDF-1. Nature medicine. 2004; 10:858–864.

Cha YR, Fujita M, Butler M, Isogai S, Kochhan E, Siekmann AF, Weinstein BM. Chemokine signaling directs trunk lymphatic network formation along the preexisting blood vasculature. Dev Cell. 2012; 22:824–836. [PubMed: 22516200]

Choi I, Chung HK, Ramu S, Lee HN, Kim KE, Lee S, Yoo J, Choi D, Lee YS, Aguilar B, et al. Visualization of lymphatic vessels by Prox1-promoter directed GFP reporter in a bacterial artificial chromosome-based transgenic mouse. Blood. 2011; 117:362–365. [PubMed: 20962325]

Davis NM, Kurpios NA, Sun X, Gros J, Martin JF, Tabin CJ. The chirality of gut rotation derives from left-right asymmetric changes in the architecture of the dorsal mesentery. Dev Cell. 2008; 15:134–145. [PubMed: 18606147]

Dotan I, Werner L, Vigodman S, Weiss S, Brazowski E, Maharshak N, Chen O, Tulchinsky H, Halpern Z, Guzner-Gur H. CXCL12 is a constitutive and inflammatory chemokine in the intestinal immune system. Inflammatory bowel diseases. 2010; 16:583–592. [PubMed: 19774645]

Feinberg RN, Noden DM. Experimental analysis of blood vessel development in the avian wing bud. Anat Rec. 1991; 231:136–144. [PubMed: 1750708]

Gallego C, Velasco M, Marcuello P, Tejedor D, De Campo L, Friera A. Congenital and acquired anomalies of the portal venous system. Radiographics: a review publication of the Radiological Society of North America, Inc. 2002; 22:141–159.

Gros J, Hu JK, Vinegoni C, Feruglio PF, Weissleder R, Tabin CJ. WNT5A/JNK and FGF/MAPK pathways regulate the cellular events shaping the vertebrate limb bud. Current biology: CB. 2010; 20:1993–2002. [PubMed: 21055947]

Hamburger V, Hamilton HL. A series of normal stages in the development of the chick embryo. 1951. Dev Dyn. 1992; 195:231–272. [PubMed: 1304821]

Hecksher-Sorensen J, Watson RP, Lettice LA, Serup P, Eley L, De Angelis C, Ahlgren U, Hill RE. The splanchnic mesodermal plate directs spleen and pancreatic laterality, and is regulated by Bapx1/Nkx3.2. Development. 2004; 131:4665–4675. [PubMed: 15329346]

Heller E, Kumar KV, Grill SW, Fuchs E. Forces generated by cell intercalation tow epidermal sheets in mammalian tissue morphogenesis. Dev Cell. 2014; 28:617–632. [PubMed: 24697897]

Heuer G. The development of the lymphatics in the small intestine of the pig. American Journal of Anatomy. 1909; 9:93–118.

Hong X, Jiang F, Kalkanis SN, Zhang ZG, Zhang XP, DeCarvalho AC, Katakowski M, Bobbitt K, Mikkelsen T, Chopp M. SDF-1 and CXCR4 are up-regulated by VEGF and contribute to glioma cell invasion. Cancer letters. 2006; 236:39–45. [PubMed: 15967572]

Huntington GS, McClure CFW. The anatomy and development of the jugular lymph sacs in the domestic cat (Felis domestica). American Journal of Anatomy. 1910; 10:177–312.

Kurpios NA, Ibanes M, Davis NM, Lui W, Katz T, Martin JF, Izpisua Belmonte JC, Tabin CJ. The direction of gut looping is established by changes in the extracellular matrix and in cell:cell adhesion. Proc Natl Acad Sci U S A. 2008; 105:8499–8506. [PubMed: 18574143]

Lortat-Jacob H. The molecular basis and functional implications of chemokine interactions with heparan sulphate. Curr Opin Struct Biol. 2009; 19:543–548. [PubMed: 19800217]

Lu MF, Pressman C, Dyer R, Johnson RL, Martin JF. Function of Rieger syndrome gene in left-right asymmetry and craniofacial development. Nature. 1999; 401:276–278. [PubMed: 10499585]

Martin SK, Diamond P, Williams SA, To LB, Peet DJ, Fujii N, Gronthos S, Harris AL, Zannettino AC. Hypoxia-inducible factor-2 is a novel regulator of aberrant CXCL12 expression in multiple myeloma plasma cells. Haematologica. 2010; 95:776–784. [PubMed: 20015878]

Matthys P, Hatse S, Vermeire K, Wuyts A, Bridger G, Henson GW, De Clercq E, Billiau A, Schols D. AMD3100, a potent and specific antagonist of the stromal cell-derived factor-1 chemokine receptor CXCR4, inhibits autoimmune joint inflammation in IFN-gamma receptor-deficient mice. J Immunol. 2001; 167:4686–4692. [PubMed: 11591799]

Mouta-Bellum C, Kirov A, Miceli-Libby L, Mancini ML, Petrova TV, Liaw L, Prudovsky I, Thorpe PE, Miura N, Cantley LC, et al. Organ-specific lymphangiectasia, arrested lymphatic sprouting, and maturation defects resulting from gene-targeting of the PI3K regulatory isoforms p85alpha, p55alpha, and p50alpha. Developmental dynamics: an official publication of the American Association of Anatomists. 2009; 238:2670–2679. [PubMed: 19705443]

Mrowicki J, Przybylowska-Sygut K, Dziki L, Sygut A, Chojnacki J, Dziki A, Majsterek I. The role of polymorphisms of genes CXCL12/CXCR4 and MIF in the risk development IBD the Polish population. Molecular biology reports. 2014; 41:4639–4652. [PubMed: 24687413]

Noden DM. Interactions and fates of avian craniofacial mesenchyme. Development. 1988; 103(Suppl): 121–140. [PubMed: 3074905]

Ny A, Autiero M, Carmeliet P. Zebrafish and Xenopus tadpoles: small animal models to study angiogenesis and lymphangiogenesis. Exp Cell Res. 2006; 312:684–693. [PubMed: 16309670]

Oliver G. Lymphatic vasculature development. Nature reviews. Immunology. 2004; 4:35–45.

Papoutsi M, Tomarev SI, Eichmann A, Prols F, Christ B, Wilting J. Endogenous origin of the lymphatics in the avian chorioallantoic membrane. Developmental dynamics: an official publication of the American Association of Anatomists. 2001; 222:238–251. [PubMed: 11668601]

Pardanaud L, Yassine F, Dieterlen-Lievre F. Relationship between vasculogenesis, angiogenesis and haemopoiesis during avian ontogeny. Development. 1989; 105:473–485. [PubMed: 2612361]

Picoli C, Nouvel V, Aubry F, Reboul M, Duchene A, Jeanson T, Thomasson J, Mouthon F, Charveriat M. Human connexin channel specificity of classical and new gap junction inhibitors. Journal of biomolecular screening. 2012; 17:1339–1347. [PubMed: 22786894]

Pilia G, Hughes-Benzie RM, MacKenzie A, Baybayan P, Chen EY, Huber R, Neri G, Cao A, Forabosco A, Schlessinger D. Mutations in GPC3, a glypican gene, cause the Simpson-Golabi-Behmel overgrowth syndrome. Nat Genet. 1996; 12:241–247. [PubMed: 8589713]

Pudliszewski M, Pardanaud L. Vasculogenesis and angiogenesis in the mouse embryo studied using quail/mouse chimeras. The International journal of developmental biology. 2005; 49:355–361. [PubMed: 15906251]

Sabin FR. On the origin of the lymphatic system from the veins and the development of the lymph hearts and thoracic duct in the pig. American Journal of Anatomy. 1902; 1:367–389.

Savin T, Kurpios NA, Shyer AE, Florescu P, Liang H, Mahadevan L, Tabin CJ. On the growth and form of the gut. Nature. 2011; 476:57–62. [PubMed: 21814276]

Shiratori H, Yashiro K, Shen MM, Hamada H. Conserved regulation and role of Pitx2 in situs-specific morphogenesis of visceral organs. Development. 2006; 133:3015–3025. [PubMed: 16835440]

Srinivasan RS, Dillard ME, Lagutin OV, Lin FJ, Tsai S, Tsai MJ, Samokhvalov IM, Oliver G. Lineage tracing demonstrates the venous origin of the mammalian lymphatic vasculature. Genes Dev. 2007; 21:2422–2432. [PubMed: 17908929]

Tachibana K, Hirota S, Iizasa H, Yoshida H, Kawabata K, Kataoka Y, Kitamura Y, Matsushima K, Yoshida N, Nishikawa S, et al. The chemokine receptor CXCR4 is essential for vascularization of the gastrointestinal tract. Nature. 1998; 393:591–594. [PubMed: 9634237]

Tamura M, Sato MM, Nashimoto M. Regulation of CXCL12 expression by canonical Wnt signaling in bone marrow stromal cells. The international journal of biochemistry & cell biology. 2011; 43:760–767. [PubMed: 21296678]

Thomason RT, Bader DM, Winters NI. Comprehensive timeline of mesodermal development in the quail small intestine. Developmental dynamics: an official publication of the American Association of Anatomists. 2012; 241:1678–1694. [PubMed: 22930586]

Uchimura K, Morimoto-Tomita M, Bistrup A, Li J, Lyon M, Gallagher J, Werb Z, Rosen SD. HSulf-2, an extracellular endoglucosamine-6-sulfatase, selectively mobilizes heparin-bound growth factors and chemokines: effects on VEGF, FGF-1, and SDF-1. BMC Biochem. 2006; 7:2. [PubMed: 16417632]

van Impel A, Zhao Z, Hermkens DM, Roukens MG, Fischer JC, Peterson-Maduro J, Duckers H, Ober EA, Ingham PW, Schulte-Merker S. Divergence of zebrafish and mouse lymphatic cell fate specification pathways. Development. 2014; 141:1228–1238. [PubMed: 24523456]

Wang J, Bai Y, Li N, Ye W, Zhang M, Greene SB, Tao Y, Chen Y, Wehrens XH, Martin JF. Pitx2-microRNA pathway that delimits sinoatrial node development and inhibits predisposition to atrial fibrillation. Proc Natl Acad Sci U S A. 2014

Welsh IC, Thomsen M, Gludish DW, Alfonso-Parra C, Bai Y, Martin JF, Kurpios NA. Integration of Left-Right Pitx2 Transcription and Wnt Signaling Drives Asymmetric Gut Morphogenesis via Daam2. Dev Cell. 2013; 26:629–644. [PubMed: 24091014]

Wigle JT, Oliver G. Prox1 function is required for the development of the murine lymphatic system. Cell. 1999; 98:769–778. [PubMed: 10499794]

Wilting J, Aref Y, Huang R, Tomarev SI, Schweigerer L, Christ B, Valasek P, Papoutsi M. Dual origin of avian lymphatics. Dev Biol. 2006; 292:165–173. [PubMed: 16457798]

Wilting J, Buttler K, Rossler J, Norgall S, Schweigerer L, Weich HA, Papoutsi M. Embryonic development and malformation of lymphatic vessels. Novartis Foundation symposium. 2007; 283:220–227. discussion 227–229, 238–241. [PubMed: 18300425]

Wilting J, Papoutsi M, Schneider M, Christ B. The lymphatic endothelium of the avian wing is of somitic origin. Developmental dynamics: an official publication of the American Association of Anatomists. 2000; 217:271–278. [PubMed: 10741421]

Witze ES, Litman ES, Argast GM, Moon RT, Ahn NG. Wnt5a control of cell polarity and directional movement by polarized redistribution of adhesion receptors. Science. 2008; 320:365–369. [PubMed: 18420933]

Yaniv K, Isogai S, Castranova D, Dye L, Hitomi J, Weinstein BM. Live imaging of lymphatic development in the zebrafish. Nature medicine. 2006; 12:711–716.

Yashiro K, Shiratori H, Hamada H. Haemodynamics determined by a genetic programme govern asymmetric development of the aortic arch. Nature. 2007; 450:285–288. [PubMed: 17994097]

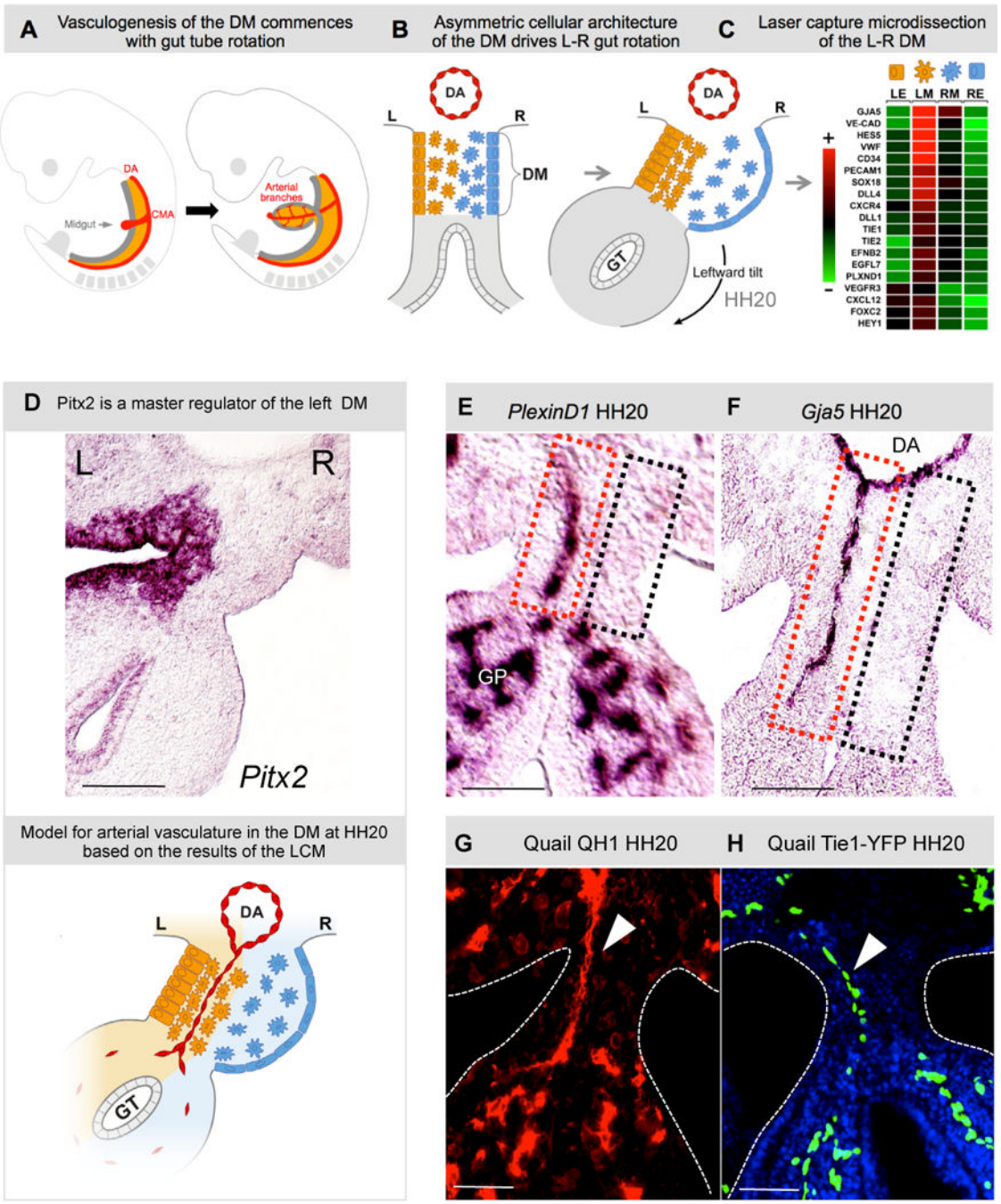

Fig. 1. Arterial development in the DM is restricted to the left side

A Midgut arteriogenesis commences at chicken HH20 (mouse E10) in the dorsal mesentery (DM, orange) concomitant with rotation of the gut tube (GT, gray), as arterial branches of the cranial mesenteric artery (CMA, a branch of dorsal aorta, DA) first connect to the gut plexus. **B** Gut tube is suspended by DM; Pitx2-drives L-R cellular asymmetries to initiate leftward rotation. **C** Heat map of L-R differentially expressed genes (LE, left epithelia; LM, left mesenchyme; RM, right mesenchyme; RE, right epithelia) in the DM leads to a model for the role of *Pitx2* (**D**, ISH, purple) in DM vascular patterning. **E,F** *PlexinD1* and *Gja5*

ISH show presence (left, red box) or absence (right, black box) of arterial D-V cords. **G,H** QH1+ and Tie1+ cords in quail embryos (arrowhead). Scale bars: **E–H** (50 μm). See also Figure S1.

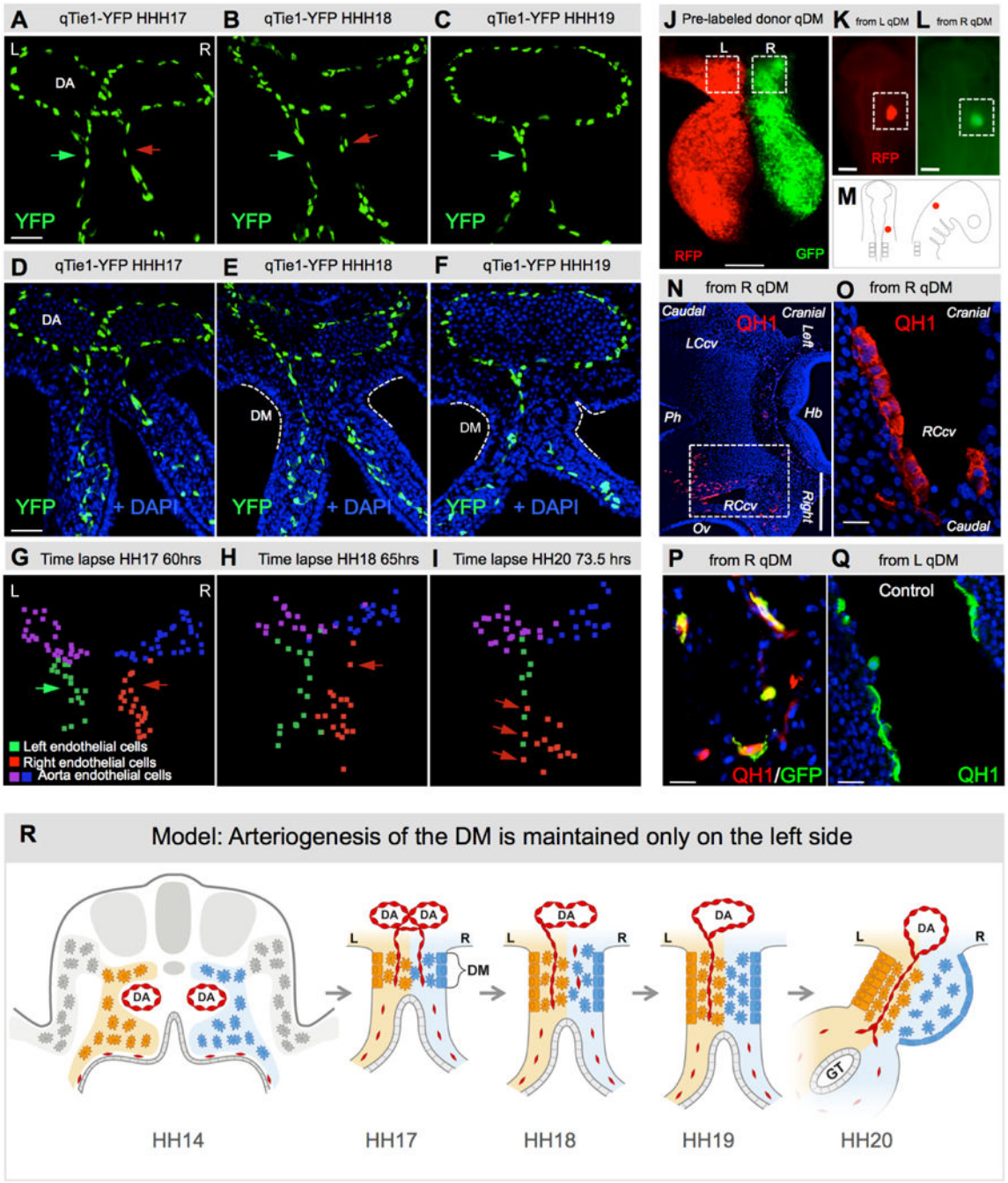

Fig. 2. The right side of the DM becomes avascular during midgut rotation

A–F Transgenic quail midgut DM transverse sections with *Tie1*:H2B-eYFP (green) and DAPI (blue) staining. **A** L-R bilateral vascular endothelial plexus is present in the DM at HH17 (green and red arrows). **B** Vascular plexus on the DM right side begins to regress (red arrow). By HH19 (**C**) the right side is avascular and only the left-sided Tie1+ D-V cords remain (green arrow). **G–I** Still frames from live time-lapse tracking of *Tie1*:H2b-eYFP cells, illustrating right-sided (red) regression of vascular endothelium. Nuclei of the left, right and the dorsal aorta endothelium are represented as green, red and blue and purple

spots, respectively (Imaris). **J–Q** Chick-quail chimera show endothelial progenitors with competence to form vessels are present on both sides of DM. **J** Dual-labeling of left (RFP) and right (GFP) donor quail DM (HH18). **K,L,M** Marked fragment is grafted onto chicken (HH9/10) where indicated, and scored at HH21 (**N–O**: Hb, hindbrain; Ov, otic vesicle; Ph, pharynx; LCcv, left cranial cardinal vein; RCcv, right cranial cardinal vein). Boxed region of **N** is magnified in **O**, where right/GFP-derived donor angioblasts (QH1, red; GFP co-stain in **P**) contribute to new vessels indistinguishable from control left/RFP-derived cells (QH1, green, **Q**). **R** Cartoon of right-sided vascular endothelial regression leading to the left-sided bias of vascular patterning in the midgut DM. Scale bars: A–F (50 μm); **J** (100 μm); **K,L** (200 μm); **N** (500 μm); **O–Q** (20 μm). See also Movies S1–3 and Fig. S2.

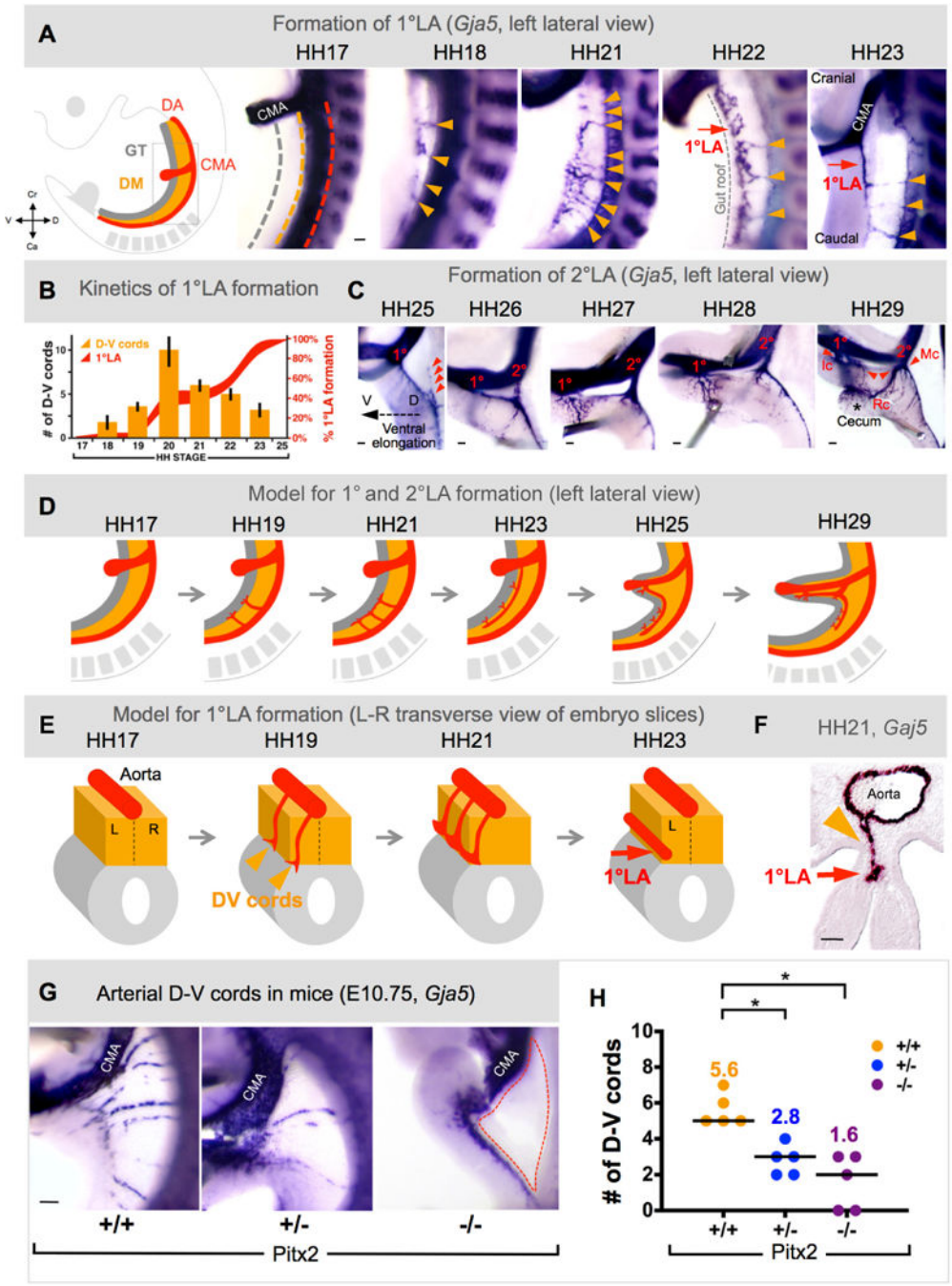

Fig. 3. Left-sided D-V cords become the major arteries supplying the midgut and are *Pitx2*-driven

A Arteriogenesis time course (1°LA formation) via wholemount ISH *(Gja5)* in chicken DM (D-V cords, orange arrows; 1°LA, red arrow), quantified in **B** (orange bars show number of D-V cords; red curves show percent longitudinal extension of 1°LA). **C** Time course (2°LA formation): 1°LA connection to CMA is established (1°, ileocolic artery, Ic) and precedes initiation of 2°LA (2°, middle colic artery, Mc) as an outgrowth of the 1°LA (red arrowheads in left panel). Subsequent anastomosis of 1° and 2° form the right colic artery

(Rc in right panel). **D,E** Model of 1° and 2°LA formation as seen from left lateral view (**D**) or in transverse (**E**). **F** Arteriogenesis in the DM initiates on the left (HH21, transverse view) where D-V cords remodel into the 1°LA **G**, Arterial cords ablated in E10.75 *Pitx2−/−* DM (dashed region); quantified in **H** (column scatter plot shows individual data and median (line); mean number is represented above each data point). Scale bars: **A** (100 μm); **C** (100 μm); **F** (50 μm); **G** (200 μm). See also Figure S3.

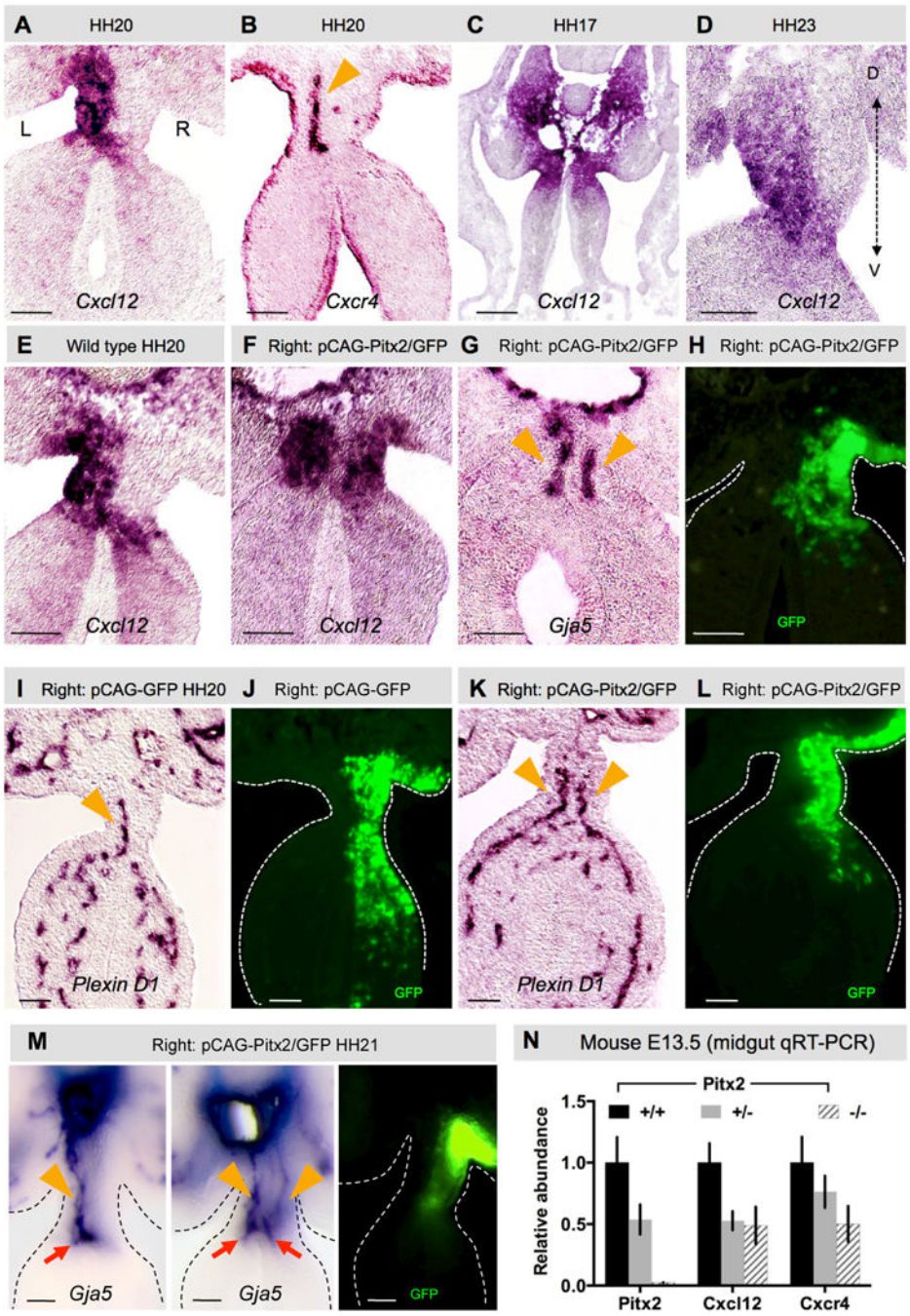

Fig. 4. Cxcr4/Cxcl12 axis is regulated by *Pitx2*

Cxcl12 (**A**) and receptor *Cxcr4* (**B**) expression in left mesenchyme and endothelial cells, respectively (ISH). **C** *Cxcl12* is bilateral (HH17) prior to DM asymmetries then (**D**) develops a left ventro-dorsal gradient (HH23). **E–L** Right DM *Pitx2* misexpression drives ectopic *Cxcl12* expression (**F** vs. **E**) and D-V arterial cords (**G**, *Gja5;* **K**, *PlexinD1*), compared to GFP-only control (**K** vs. **I**; GFP (**H,J,L**) labels electroporated cells). Orange arrowheads mark arterial cords (**B,G,I,K**). **M** 'Double left' vascular phenotype upon right-sided Pitx2 misexpression (orange arrowheads point to D-V cords, red arrows point to

1°LA). **N** Relative expression levels of Cxcl12 and Cxcr4 in E13.5 *Pitx2−/−* DM. Scale bars are 50 μm. See also Figure S4.

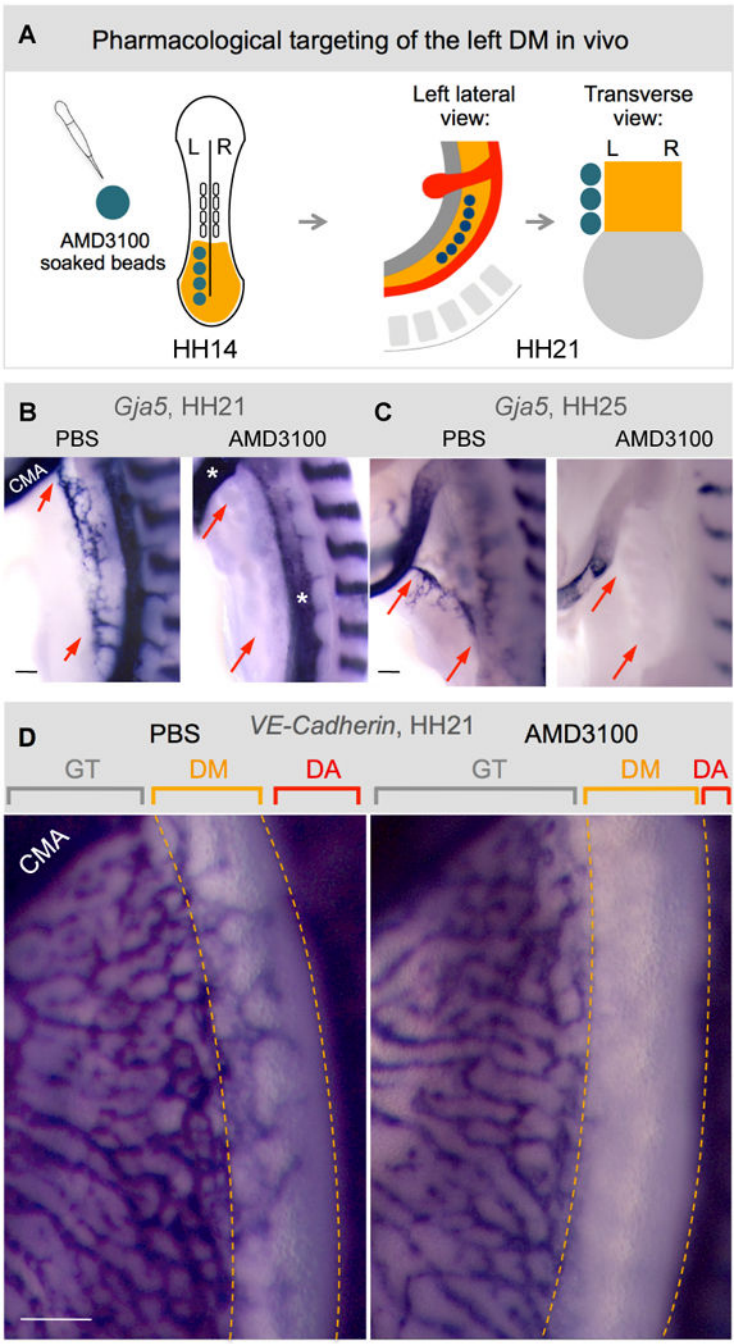

Fig. 5. The Cxcr4/Cxcl12 axis is necessary for arterial vascular development in the DM

A Targeting of the left DM with AMD3100. Beads are placed into the left coelomic cavity (HH14) prior to DM formation to target splanchnic mesoderm. Beads remain intact at HH21 when embryos are analyzed. Compared to PBS-control beads (**B–D**), AMD3100-beads ablate left arterial cords (**B**, HH21, ISH *Gja5*, red arrows) and 1°LA (**C**, HH25, red arrows), but leave adjacent gut vascular plexus, CMA, and DA, unaffected (**D**, *VE-cadherin*, HH21). CMA, cranial mesenteric artery; GT, gut tube; DA, dorsal aorta. Scale bars are 100 μm. See also Figure S5.

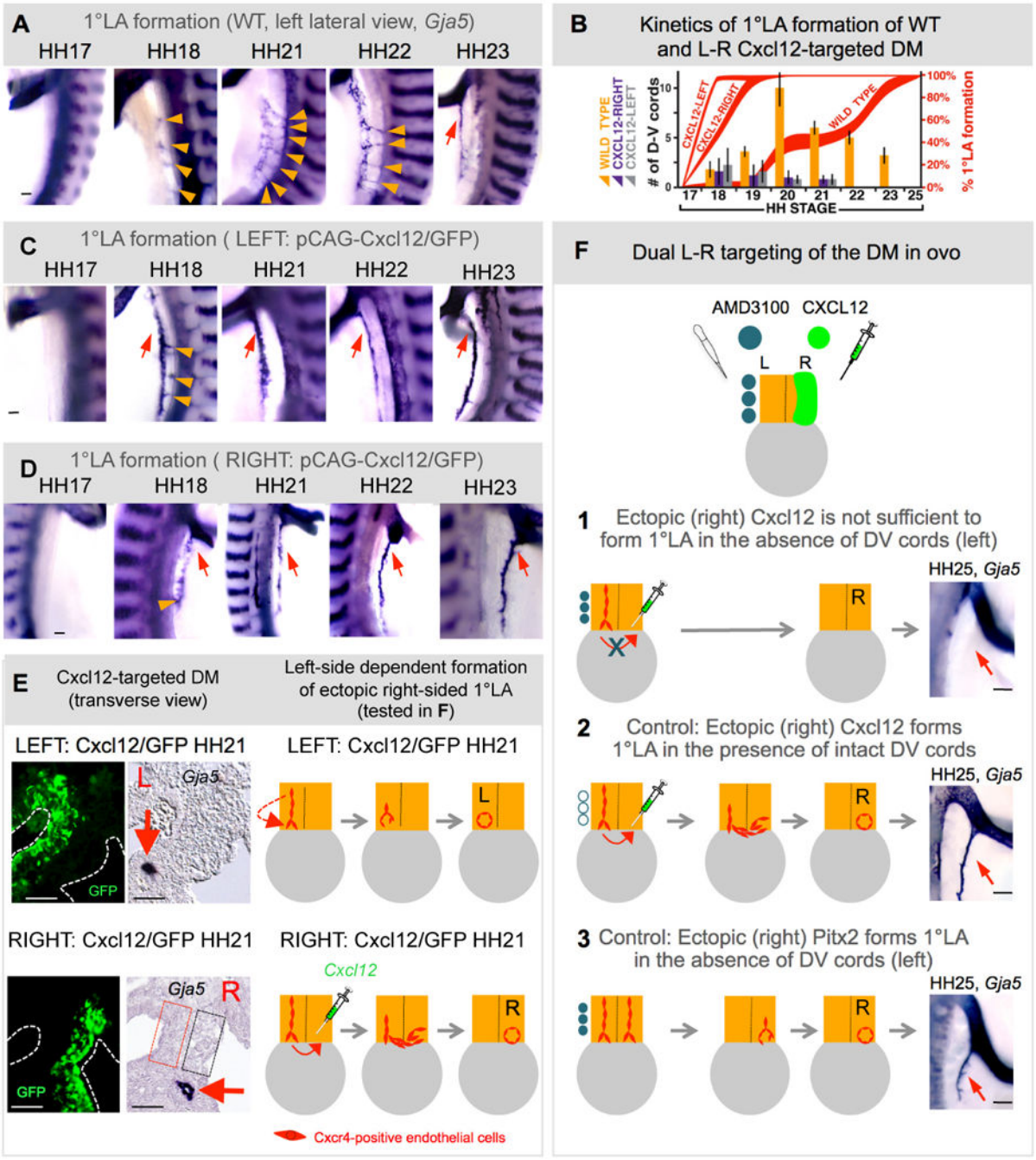

Fig. 6. Cxcl12 expression is not sufficient to drive D-V cord formation in the absence of Pitx2

A–E Exogenous left (or right) *Cxcl12* expression accelerates left-sided D-V remodeling and 1°LA formation. **A** Lateral views of DM arteriogenesis in WT, left-side (**C**) and right-side (**D**) *Cxcl12* electroporated embryos (Wholemount ISH *Gja5*), quantified in **B** (bars show number of D-V cords, red curves show percent longitudinal extension of 1°LA). **E** Transverse sections of left-side (**top**) or right-side (**bottom**) *Cxcl12* electroporated embryos (*Gja5* ISH, GFP labels targeted cells) show left-sided (**top**) or right-sided (**bottom**) location bias in the formation 1°LA (red arrow). Dashed boxes mark the presumptive location of the

normal left-sided (red) and ectopically formed right-sided (black) D-V arterial cords. Cartoon shows proposed model for the left-side dependent formation of the ectopic right-sided 1°LA, tested in a dual L-R targeting experiment in **F**. DM dual targeting (HH25, wholemount ISH *Gja5*, right lateral view of embryos, summarized in cartoons): (**1**) left-sided AMD3100-soaked beads with right-sided *Cxcl12;* (**2**) PBS beads and right-sided *Cxcl12*; or (**3**) left-sided AMD3100 beads with right-sided *Pitx2* (bottom) demonstrate the requirement of the left side for 1°LA formation. Scale bars: **A,C,D** (100 μm); **E** (50 μm); **F** (100μm). See also Figure S6.

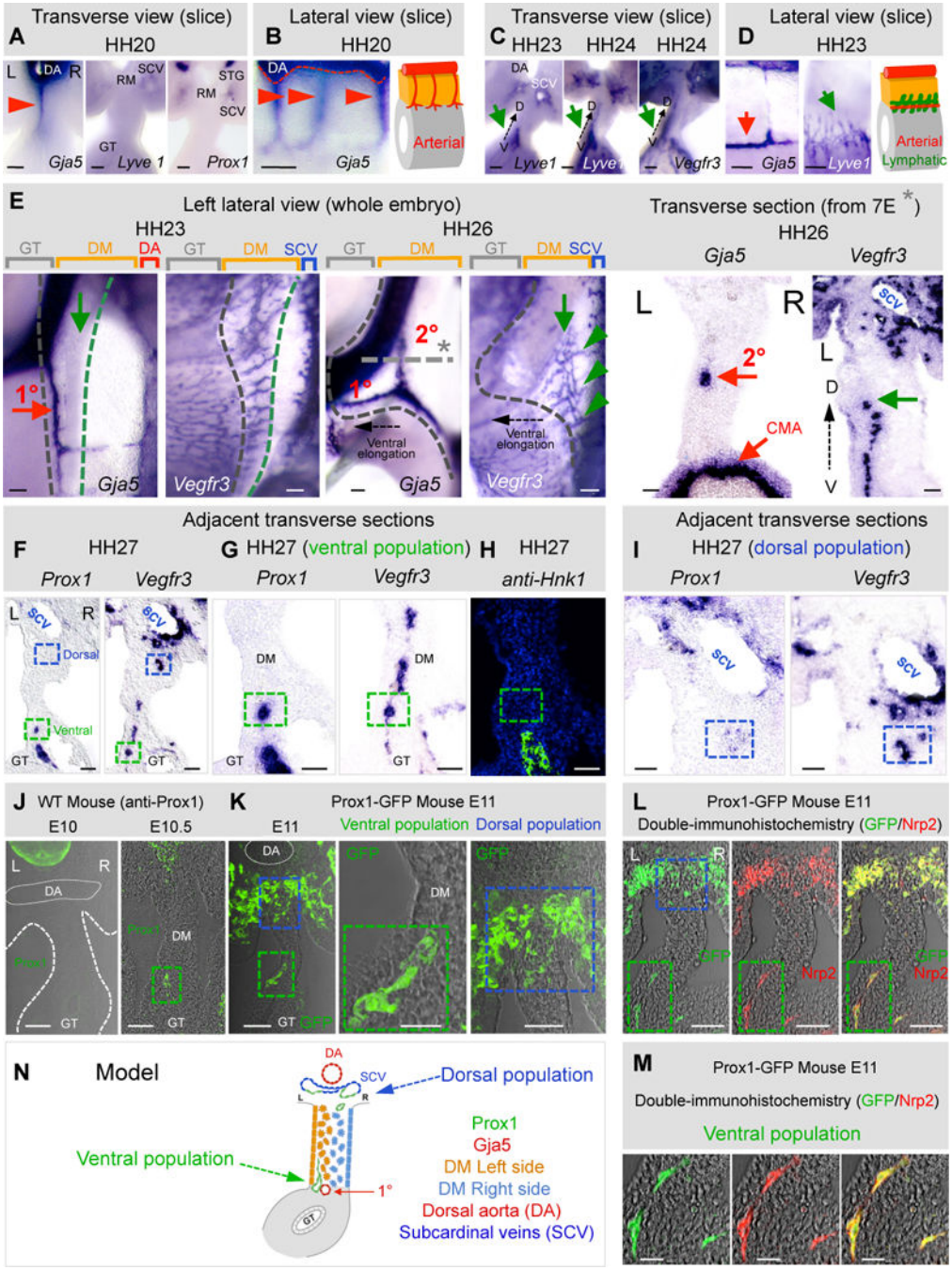

Fig. 7. Lymphangiogenesis in the DM is left-sided and initiates locally

ISH during DM arteriogenesis with probes specific for arterial (*Gja5*) and lymphatic (*Lyve1*, *Vegfr3*, and *Prox1*) markers: transverse (**A,C,E right column, F–I**) and lateral views (**B,D,E**) of DM/gut tube vibratome slices (**B,C,D**) or wholemount embryos (**E**) and transverse sections (**E**). **A,B** At HH20 only arterial cords are present (red arrowhead and cartoon). **C,D** At HH23–24, *Lyve1* and *Vegr3* mark lymphatics in the ventral left DM (**C,D**, green arrows; **D**, cartoon) while 1°LA has formed (red arrow). **E** Left lateral views, HH23 showing lymphatic field (green arrow, *Vegfr3*) forming along the 1°LA (red arrow, *Gja5*).

Lymphatic field (green arrow) at HH26 moves dorsally and parallels the 2°LA now formed (green arrowheads show dorsal connections of the lymphatic field with the SCV). Gray dashed line/asterisk marks location of transverse section. Black dashed arrow shows ventral elongation of the midgut loop. Transverse sections of ISH showing left-sided location of the 2°LA (*Gja5*) and lymphatic field (*Vegfr3*). **F** Distinct ventral (green box) and dorsal (blue box) populations of chicken DM lymphatics, revealed by *Prox1* and *Vegfr3* ISH on adjacent sections; higher magnifications: ventral (**G**) and dorsal (**I**) domains. **H** Prox1+ avian Nerve of Remak in the ventral domain stains Hnk1+, distinct from Prox1+, Hnk1− lymphatics (green box). **JK** Distinct lymphatic populations (E10–11) in WT mice (**J**, anti-Prox1) and in Prox1-GFP transgenic mice (**K**, anti-GFP). LM Double-IH of Prox1-GFP mice with Nrp2 (**M** shows higher magnification of ventral population from **L**) **N** Cartoon model summary of ventral left and dorsal lymphatic populations. Scale bars: **A–D, E right column, I,J,K (left, right panels), L, M** (50 μm); **E left column, F,G,H** (100 μm); **K (middle panel)** (20 μm). See also Figure S7.

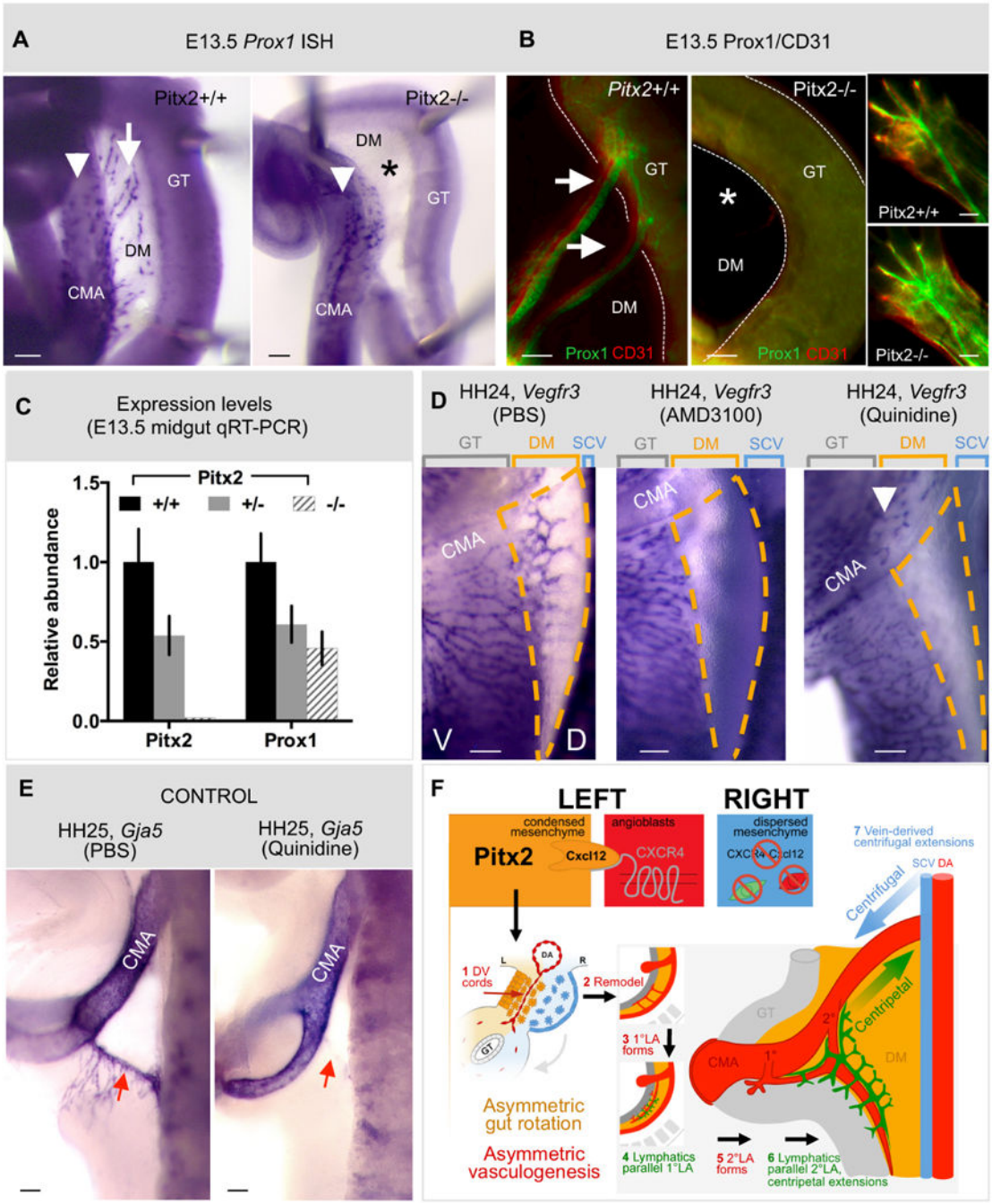

Fig. 8. Local lymphangiogenesis in the left DM requires the preceding arterial program, driven by Pitx2

A,B Prox1+ mesenteric lymphatic vessels (white arrows, Pitx2+/+) are absent in embryos lacking *Pitx2* (asterisk in Pitx2−/− panels), as revealed by **(A)** wholemount ISH and **(B)** immunostaining for Prox1/CD31 at E13.5 in the mouse. Prox1+ cells alongside the CMA wall (white arrowhead in **A**) or of dermal lymphatics (**B**, insets) are unaffected by *Pitx2* loss. **C** Quantitative RT-PCR reveals loss of Prox1 expression in whole gut isolates of Pitx2 +/− and Pitx2−/− mouse embryos. **D** Compared to PBS (left panel), the DM (orange dashed

regions) is devoid of lymphatic vessels (ISH *Vegfr3*) upon pharmacological inhibition of arteriogenesis, either targeting Cxcr4 (AMD3100, middle panel) or Gja5/Cx43 (quinidine, right panel). **E** Confirmation that arteries (ISH *Gja5*) in the DM are lost upon quinidine treatment (right panel) compared to PBS controls (left panel). **F** Proposed model: Pitx2 directs *Cxcl12* in the left DM. This induces endothelial chemotaxis via Cxcr4 and D-V cord formation, remodeling and formation of CMA arterial branches. A lymphatic plexus initiates in the ventral left DM and, via centripetal extension, connects with centrifugal branches of the systemic lymphatics of venous descent. Scale bars are 100 μm. See also Figure S8.